ORIGINAL RESEARCH

Inhibition of Regulatory-Associated Protein of Mechanistic Target of Rapamycin Prevents Hyperoxia-Induced Lung Injury by Enhancing Autophagy and Reducing Apoptosis in Neonatal Mice

Angara Sureshbabu[1]*, Mansoor Syed[1,2], Pragnya Das[2], Cecilia Janér[3], Gloria Pryhuber[4], Arshad Rahman[4], Sture Andersson[3], Robert J. Homer[5], and Vineet Bhandari[1,2]

[1]Division of Perinatal Medicine, Department of Pediatrics, Yale University School of Medicine, New Haven, Connecticut; [2]Section of Neonatal–Perinatal Medicine, Department of Pediatrics, Drexel University College of Medicine, Philadelphia, Pennsylvania; [3]Children's Hospital, University of Helsinki, Helsinki, Finland; [4]Department of Pediatrics, University of Rochester School of Medicine and Dentistry, Rochester, New York; and [5]Department of Pathology, Yale University School of Medicine, New Haven, Connecticut

Abstract

Administration of supplemental oxygen remains a critical clinical intervention for survival of preterm infants with respiratory failure. However, prolonged exposure to hyperoxia can augment pulmonary damage, resulting in developmental lung diseases embodied as hyperoxia-induced acute lung injury and bronchopulmonary dysplasia (BPD). We sought to investigate the role of autophagy in hyperoxia-induced apoptotic cell death in developing lungs. We identified increased autophagy signaling in hyperoxia-exposed mouse lung epithelial-12 cells, freshly isolated fetal type II alveolar epithelial cells, lungs of newborn wild-type mice, and human newborns with respiratory distress syndrome and evolving and established BPD. We found that hyperoxia exposure induces autophagy in a *Trp53*-dependent manner in mouse lung epithelial-12 cells and in neonatal mouse lungs. Using pharmacological inhibitors and gene silencing techniques, we found that the activation of autophagy, upon hyperoxia exposure, demonstrated a protective role with an antiapoptotic response. Specifically, inhibiting regulatory-associated protein of mechanistic target of rapamycin (RPTOR) in hyperoxia settings, as evidenced by wild-type mice treated with torin2 or mice administered (*Rptor*) silencing RNA via intranasal delivery or $Rptor^{+/-}$, limited lung injury by increased autophagy, decreased apoptosis, improved lung architecture, and increased survival. Furthermore, we identified increased protein expression of phospho-beclin1, light chain-3-II and lysosomal-associated membrane protein 1, suggesting altered autophagic flux in the lungs of human neonates with established BPD. Collectively, our study unveils a novel demonstration of enhancing autophagy and antiapoptotic effects, specifically through the inhibition of RPTOR as a potentially useful therapeutic target for the treatment of hyperoxia-induced acute lung injury and BPD in developing lungs.

Keywords: cell death; oxygen; newborn; pulmonary; bronchopulmonary dysplasia

Premature infants provided with supplemental oxygen are at higher risk for developing a chronic respiratory disease, bronchopulmonary dysplasia (BPD) (1). BPD occurs in developing lungs resulting in impaired alveolarization and dysregulated vascularization—the pathologic hallmarks (2). Premature infants diagnosed with BPD have diminished pulmonary function and reduced lung capacity as they grow older and up to adulthood (3). This disease represents a common yet complicated clinical issue associated with significant long-term morbidity and mortality (2, 3). Pulmonary-specific oxygen toxicity is

(Received in original form October 28, 2015; accepted in final form June 17, 2016)

*Present affiliation: Department of Medicine, Division of Pulmonary and Critical Care Medicine, Weill Cornell Medicine, Cornell University, New York, NY.

This work was supported in part by National Heart, Lung, and Blood Institute (NHLBI)/National Institutes of Health (NIH) grants HL63039 (G.P.) and HL116632 (A.R.), by the Sigrid Jusélius Foundation (S.A.), and by NHLBI/NIH grant HL85103 (V.B.).

Author Contributions: Concept and design—A.S. and V.B.; acquisition of data—A.S., M.S., P.D., C.J., G.P., A.R., S.A., R.J.H., and V.B.; data analysis and interpretation—A.S., M.S., P.D., C.J., G.P., A.R., S.A., R.J.H., and V.B.; drafting and/or critical revision for intellectual content—A.S., M.S., P.D., C.J., G.P., A.R., S.A., R.J.H., and V.B.; all authors have approved the version of the submitted manuscript.

Correspondence and requests for reprints should be addressed to Vineet Bhandari, M.D., D.M., Department of Pediatrics, Drexel University College of Medicine, New College Building, 245 North 15th Street, Philadelphia, PA 19102. E-mail: vineet.bhandari@drexelmed.edu

This article has an online supplement, which is accessible from this issue's table of contents at www.atsjournals.org

Am J Respir Cell Mol Biol Vol 55, Iss 5, pp 722–735, Nov 2016

Originally Published in Press as DOI: 10.1165/rcmb.2015-0349OC on July 2, 2016
Internet address: www.atsjournals.org

Clinical Relevance

The inability to treat neonatal lung diseases is due to the presence of significant unknowns in the field. This research identified inhibition of regulatory-associated protein of mechanistic target of rapamycin as a potentially therapeutic target for the treatment of hyperoxia-induced acute lung injury (HALI) and bronchopulmonary dysplasia (BPD). This study demonstrated increased expression of phospho-beclin1, light chain-3-II, and lysosomal-associated membrane protein 1 in human lung tissues of premature infants with diseases characterized by HALI (i.e., respiratory distress syndrome and BPD).

usually referred to as hyperoxia-induced acute lung injury (HALI). Prolonged delivery of high concentrations of oxygen to infants results in HALI and BPD (1, 4). However, the mechanisms related to HALI and BPD are poorly understood.

Macroautophagy (hereafter referred as autophagy) is an evolutionarily conserved, intracellular catabolic process where the cell self-cannibalizes long-lived proteins, protein aggregates, and dysfunctional organelles in a lysosomal-dependent manner during stressful conditions, such as starvation, hypoxia, and infection. Autophagy is mediated by distinct molecular events, which broadly include isolation membrane/phagophore formation, vesicle nucleation, fusion of autophagosome with lysosome, and degradation (5). Numerous lines of experimental data have shown that autophagy can be activated in response to a myriad of physical and chemical stresses (6). Stress regulated autophagy can also occur under normal homeostatic conditions when nutrients are not a limiting factor (7). Autophagy is actively induced in almost all tissues, except the brain, during the early neonatal period. The importance of autophagy in development can be assessed from the fact that deletion of essential autophagy genes (beclin [BECN] 1, autophagy-related [ATG] 5) in mice causes early embryonic or neonatal lethality (5). The role of autophagy in development is clearly important, but its role and contribution to hyperoxia-induced injury

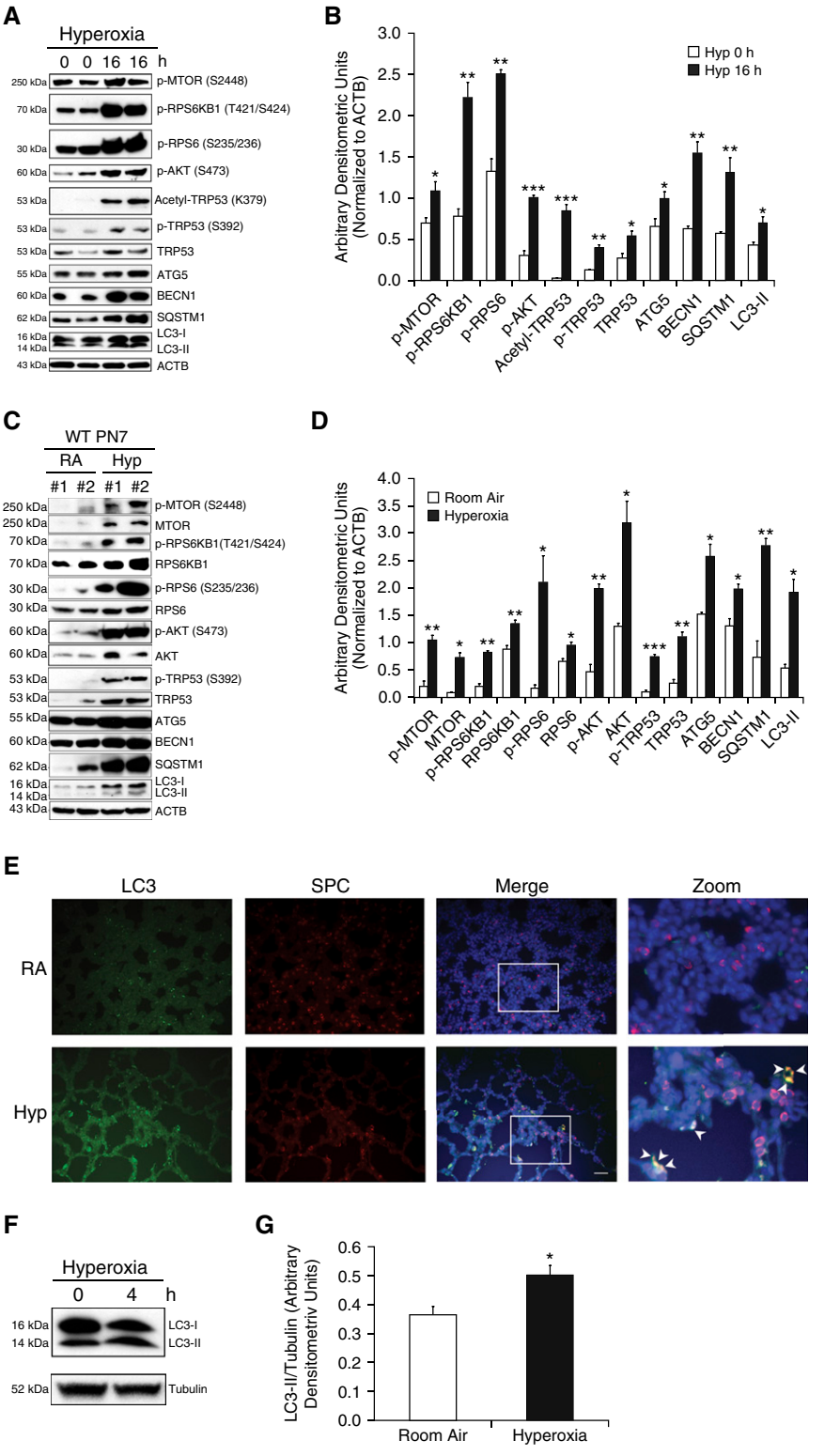

Figure 1. Hyperoxia induces autophagy in lung epithelial cells and neonatal mouse lungs. (*A*) Mouse lung epithelial (MLE)-12 cells were incubated with or without the presence of hyperoxia (95% O_2 + 5% CO_2) for 16 hours. Western blot analysis showed up-regulation of phospho-MTOR (p-MTOR), phospho-ribosomal protein S6 kinase beta-1 (p-RPS6KB1), phospho-RPS6 (p-RPS6), phospho-Akt (p-Akt), acetyl-transformation–related protein (TRP) 53, phospho-TRP53 (p-TRP53), and TRP53 with concomitant increased expression of autophagy-related (ATG) 5, beclin (BECN) 1, sequestosome 1

in developing lungs is currently unknown. On the other hand, autophagy has been reported to inhibit or promote cell death both in developmental and diseased conditions (5). Thus, we attempted to study the role of autophagy signaling pathway in hyperoxia-induced injury in developing lungs.

The mechanistic target of rapamycin (MTOR) is a Ser/Thr protein kinase complex pathway that regulates cell growth and proliferation in response to energy levels, nutrients, and hormones. MTOR is a catalytic subunit of two distinct complexes, namely, MTOR complex (MTORC) 1 and MTORC2. Regulatory-associated protein of MTOR, complex 1 (RPTOR) is a major subunit found in MTORC1, but not in MTORC2. MTORC1 is a negative regulator of autophagy by regulating the activity of Unc-51 like autophagy activating kinase 1 (ULK1) complex that is essential for the formation of autophagosomes (8).

Herein, we first identified the up-regulation of the autophagy pathway in newborn (NB) mouse lung tissues and type II alveolar epithelial cells (AECs) exposed to hyperoxia. We also characterized the role of autophagy in the context of HALI and BPD. Our results provide evidence that hyperoxia activates formation of autophagosomes and increases fusion between autophagosomes and lysosomes in a *Trp53*-dependent manner. This degradative autophagy has a protective role, as it limits alveolar lung epithelial cell death. Furthermore, inhibiting RPTOR, a key component of MTORC1, led to increased autophagy, decreased apoptosis, and improved lung architecture in hyperoxia settings. We also demonstrated clinical relevance by showing increased expression of phospho-BECN1, light chain-3 (LC3)-II, and lysosomal-associated membrane protein (LAMP) 1 in human lung tissues of premature infants with diseases characterized by HALI (i.e., respiratory distress syndrome [RDS] and BPD).

Materials and Methods

Additional details of materials and methods are provided in the online supplement.

Chemicals/Reagents

The chemicals used in the experiments included chloroquine diphosphate (CQ; catalog no. C6628; Sigma-Aldrich, St. Louis, MO), Pifithrin-α (catalog no. P4359; Sigma) and Torin2 (catalog no. 4,248; Tocris Bioscience, Bio-Techne, Minneapolis, MN). All other chemicals, antibodies, solvents, and reagents used were obtained from commercially available sources.

Cell Culture

Tissue culture media and fetal bovine serum were obtained from Invitrogen Inc. (Grand Island, NY). Mouse lung epithelial (MLE)-12 cells, (no. CRL-2210; ATCC, Manassas, VA), a generous gift from Patty J. Lee, M.D. (Yale University, New Haven, CT), were maintained in Dulbecco's modified Eagle medium supplemented with 2% vol/vol fetal bovine serum, 100 U/ml penicillin, 100 μg/ml streptomycin at 37°C in 95% air, 5% CO_2 atmosphere.

Type II AECs Isolation

Type II AECs were isolated from fetuses of Embryonic Day (E) 19–E20 female adult mice. The isolation procedure was performed according to a modified protocol (9).

siRNA Transfection

Mouse *Atg5*, *Becn1*, *Map1lc3/Lc3*, and *Lamp1* silencing RNAs were purchased from Applied Biosystems (Life Technologies, Carlsbad, CA). Mouse SMARTpool on-Target plus *Trp53* siRNAs were purchased from Thermo Fisher Scientific Inc. (Pittsburgh PA). MLE-12 cells were first transfected with respective siRNAs using transfection reagents (catalog no. 13778-075 for *Atg5*, *Becn1*, *Lc3*, *Lamp1* siRNAs; catalog no. T-2001-02 for *Trp53* siRNA; Thermo Fisher Scientific). Then, cells were exposed to hyperoxia using recommended media, per the indicated time points. Next, cells were lysed for protein extraction and samples were subjected to the Western blot procedure.

Dead/Live Cell Fluorescence Assay

After timed hyperoxia exposure, MultiTox fluor multiplex cytoxicity assay (catalog no. G9201; Promega, Madison, WI) was performed according to the manufacturer's instructions using Glomax Multiplex plate reader (Promega).

Animals

C57BL/6 mice were used. During hyperoxia survival experiments, all NB mice were exposed to 100% O_2 with two lactating dams being used and alternated every 24 hours between room air and hyperoxia to ensure sufficient nutrition (milk) for indicated time points, as previously described (10, 11). *Rptor* flox/flox (B6. *Cg-Rptor*$^{tm1.1Dmsa}$/J) and *Nkx*2.1 Cre (C57BL/6J-Tg(*Nkx*2–1-cre)2Sand/J) mice were purchased from Jackson Laboratory (Bar Harbor, ME). Throughout the experiments, mice were given free access to food and water.

RNA Interference Analysis

For *Mtorc1* silencing purposes, animal grade *Rptor* and *Trp53* siRNAs were purchased from Applied Biosystems (Life Technologies).

Lung Morphometry

Alveolar size was estimated from the mean chord length of the airspace and septal thickness, as described previously (10, 11).

Figure 1. (Continued). (SQSTM1), and light chain-3 (LC3)-II proteins. (*B*) Densitometric analysis was performed and the expression of observed proteins was normalized to β-actin. (*C*) Newborn (NB) wild-type (WT) mice were exposed to hyperoxia from Postnatal Days (PNs) 1–7. Western blots showing increased expression of phospho-MTOR, MTOR, phospho-RPS6KB1, RPS6KB1, phospho-RPS6, RPS6, phospho-AKT, AKT, phopsho-TRP53, TRP53, and also increased expression of ATG5, ATG7, SQSTM1, and LC3-I/-II proteins in lung tissues. (*D*) Densitometric analysis was performed, and the expression of observed proteins was normalized to β-actin. (*E*) Representative immunofluorescent images depicting colocalization of pro–surfactant protein-C (*red*) and LC3 proteins (*green*) in serial sections of hyperoxia-exposed lungs obtained from NB WT mice. *Inset images* were enlarged, indicating co-localization (*yellow*) of LC3 in type II alveolar epithelial cells (AECs), as denoted by the *arrowheads*. (*F* and *G*) Western blot analysis demonstrating increased expression of LC3-II (normalized to α-tubulin) in hyperoxia-exposed Embryonic Day (E) 19–20 freshly isolated type II AECs for 4 hours. Values are means ± SEM of a minimum of three independent experiments (*in vitro*) or four animals in each group (*in vivo*). $^{*}P < 0.05$, $^{**}P < 0.01$, $^{***}P < 0.001$, compared with respective controls. ACTB, β-actin; Hyp, hyperoxia; MTOR, mechanistic target of rapamycin; RA, room air; SPC, surfactant protein C.

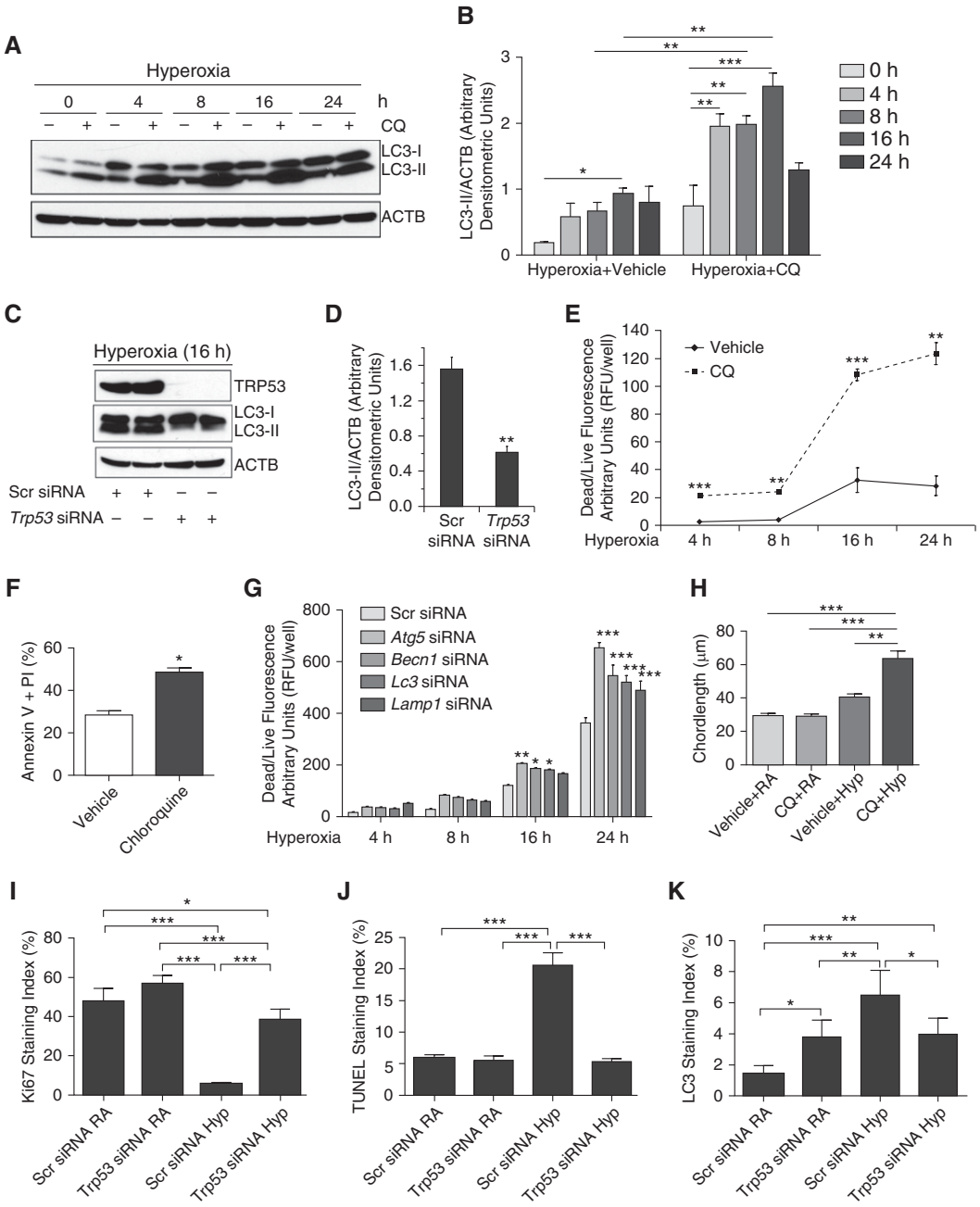

Figure 2. Hyperoxia-induced autophagic flux prevents cell death in a TRP53-dependent manner in MLE cells. (*A*) MLE-12 cells were pretreated with or without chloroquine (CQ; 25 μM) for 1 hour and exposed to hyperoxia in a time course–dependent manner. Western blot image showing increased LC3-II expression at a rate of function of time in the presence of CQ compared with matched controls. (*B*) Densitometric analysis showing significantly increased ratio of LC3-II to β-actin and represented as a *bar graph*. (*C*) MLE-12 cells were pretreated with a pool of *Trp53* silencing RNAs (siRNAs) and exposed to hyperoxia. *Trp53*-knockdown MLE-12 cells showed decreased LC3-II expression as compared with a scrambled (Scr) pool of siRNA controls. (*D*) Densitometric analysis showing significantly decreased LC3-II:β-actin ratio in *Trp53* siRNA–treated sample as compared with Scr siRNA–treated control. (*E*) MLE-12 cells were treated with or without CQ (25 μM) and exposed to hyperoxia, and dead/live cell fluorescence assay was performed at indicated time points. (*F*) MLE-12 cells were treated with CQ and exposed to hyperoxia for 16 hours and subjected to annexin V and propidium iodide (PI) assay. Representative *bar graph* showing significantly increased FACS analysis of cells staining positive for annexin V and PI in the CQ-treated group compared with its control. (*G*) MLE-12 cells were treated with *Atg5*, *Becn1*, *Map1lc3a*, and lysosomal-associated membrane protein 1 (*Lamp1*) siRNAs (20 μM) and exposed to hyperoxia for indicated time points. *Bar graph* showing significantly increased dead/live cell fluorescence in hyperoxia-exposed MLE-12 cells treated with *Atg5*, *Becn1*, *Map1lc3a*, and *Lamp1* siRNAs at the 24-hour time point. (*H*) Morphometric analysis of lung histology sections of NB WT mice exposed to RA or survived 100% O_2 at PN7. (*I–K*) Ki67, terminal deoxynucleotidyl transferase dUTP nick end labeling (TUNEL), and LC3 staining indices of *Trp53* siRNA–treated WT PN4 mice exposed to hyperoxia as compared with the Scr siRNA group. Values are means ± SEM of a minimum of three independent experiments (*in vitro*) or four animals (*in vivo* experiments). $^{*}P < 0.05$, $^{**}P < 0.01$, $^{***}P < 0.001$, ANOVA. RFU, relative fluorescence units.

Pulmonary Arterial Hypertension–Induced Right Ventricular Hypertrophy

Quantitative measurements of pulmonary arterial hypertension (PAH)–induced right ventricular (RV) hypertrophy (RVH) by RV/left ventricle and RV/(left ventricle + interventricular septum) ratios were done using the methodology described previously (12).

Statistical Analyses

Values are expressed as mean (±SEM). Groups were compared with the Student's two-tailed unpaired *t* test or one-way ANOVA (followed by Tukey's multiple comparison *post hoc* test) or two-way ANOVA as appropriate (followed by Bonferroni's multiple comparison *post hoc* test), using GraphPad Prism 5.0 (GraphPad Software, Inc., San Diego, CA). A value of *P* less than 0.05 was considered statistically significant.

Results

Hyperoxia Induces Autophagy in Lung Epithelial Cells and Neonatal Mouse Lungs

Autophagy has recently been implicated in the regulation of hyperoxia-induced epithelial cell death (13). The hallmark of autophagy lies in the conversion of LC3-I activated by ATG7, transferred to ATG3, and conjugated to phosphatidyl-ethanolamine at the outer and inner autophagosomal membrane to form LC3-II (13). Although LC3-II increase is considered a standard marker of autophagy activation, it is important to assess the multiple components of the signaling pathway and the autophagic flux (14). Downstream blockers for the fusion of autophagosome and lysosome include chemical inhibitors, such as CQ (15). Under the latter circumstance, increased LC3-II expression is expected.

To define the relationship between hyperoxia exposure and autophagy, we first looked at the protein expression of autophagy signaling. Exposure to hyperoxia in MLE-12 cells led to the activation of autophagy markers (Figure 1A), which was confirmed by densitometry (Figure 1B). To assess the *in vivo* relevance of the autophagy pathway in HALI in developing lungs, we next exposed NB wild-type (WT) mice to hyperoxia from Postnatal Day (PN) 1 to PN7. In accordance with our *in vitro* results, we noted activation of the autophagy markers (Figure 1C), confirmed by densitometry (Figure 1D). Furthermore, we showed colocalization of LC3 and surfactant protein C (SPC) in relevance to type II AECs in NB WT PN7 mice exposed to hyperoxia (Figure 1E). In line with this, we noted increased expression of LC3-II/tubulin in freshly isolated type II AECs from E19–E20 fetal mouse lungs, on exposure to 4 hours of hyperoxia (Figures 1F and 1G). In addition to autophagy markers, we also noted transformation-related protein (TRP) 53 activation and increased activity of MTORC1 and MTORC2 both in MLE-12 cells and NB WT PN7 mouse lungs (Figures 1A–1D).

Hyperoxia-Induced Autophagy Prevents Cell Death in a *Trp53*-Dependent Manner *In Vitro*

The increase in LC3-II could be a result of increased number of autophagosomes only. However, for the autophagy process to be completed, the autophagosome needs to fuse with the lysosome to form the autolysosome for final degradation. To confirm the autophagic flux, we used CQ, an inhibitor of autophagy, specifically known to block the autolysosomal acidification and, therefore, to prevent the fusion between autophagosome and lysosome (15). As noted in Figures 2A and 2B, MLE-12 cells pretreated with CQ (25 μM) and exposed to hyperoxia were noted to have a significant increase in LC3-II expression compared with appropriate controls. To examine the relationship between TRP53 and autophagy pathways, *Trp53* knockdown experiments were performed using specific siRNA in MLE-12 cells and subjected to hyperoxia. As noted in Figures 2C and 2D, loss of *Trp53* inhibited LC3-II expression in hyperoxic conditions. Furthermore, pifithrin-α (a known TRP53 inhibitor) treatment resulted in decreased LC3-II expression upon hyperoxia exposure to MLE-12 cells (*see* Figure E1 in the online supplement).

To investigate the role of autophagy in cell death in hyperoxia settings, we used the autophagy inhibitor, CQ, a 4-aminoquinoline drug that inhibits lysosomal acidification (15). As shown in Figure E2 and Figures 2E and 2F, CQ treatment (25 μM) led to a significant increase in apoptotic cell death in hyperoxia-exposed MLE-12 cells. To delineate the signaling pathway of this response, we used siRNAs targeted to *Atg5* (a marker for autophagosome onset; Figure E3A), *Becn1* (a marker for the initial nucleation step of autophagosome; Figure E3B), *Map1lc3/Lc3* (marker of autophagosome; Figure E3C), or *Lamp1* (a marker for the fusion between autophagosome and lysosome; Figure E3D). Inhibition of specific aspects of the signaling process of autophagy led to increased cell death (Figure 2G). These data suggest that hyperoxia increases autophagic flux and prevents apoptotic cell death in a *Trp53*-dependent manner in lung epithelial cells.

To assess the *in vivo* relevance of our *in vitro* findings, we next treated NB WT mice with CQ with concomitant exposure to hyperoxia from PN1 to PN7, with appropriate controls. CQ treatment with hyperoxia worsened the pulmonary phenotype, with evidence of larger, simplified alveoli with thinner walls, confirmed by quantitative assessment using chord length (Figures 2H and Figure E8A). Furthermore, the pulmonary phenotype was associated with increased expression of proapoptotic markers (active BAX, and cleaved caspase [CASP] 3) and decreased antiapoptotic BCL2 (Figure E4).

In addition, to evaluate the contribution of *Trp53 in vivo*, we used siRNA delivery to hyperoxia-exposed neonatal mice, and assessed the response (Figures 2I–2K; Figures E8B–E8D). We noted that the cell proliferation marker, Ki67, was significantly increased in the *Trp53* siRNA–treated hyperoxia group in WT PN4 mice as compared with scrambled siRNA–treated hyperoxia-exposed WT PN4 mice (Figure 2I). Terminal deoxynucleotidyl transferase dUTP nick end labeling staining index significantly decreased in the *Trp53* siRNA–treated hyperoxia-exposed group as compared with scrambled siRNA–treated hyperoxia-exposed WT PN4 mice (Figure 2J). Importantly, the autophagy marker LC3-II staining index significantly decreased in the *Trp53* siRNA–treated hyperoxia-exposed group as compared with scrambled siRNA–treated hyperoxia-exposed WT PN4 mice (Figure 2K). This would suggest

that the autophagy pathway is regulated partly by *Trp53*, but not exclusively in terms of the concomitant apoptotic response, as we noted a decrease in apoptosis. However, we cannot rule out a dose response, as the *Trp53* siRNA decreased the protein levels by approximately 50% (Figures E8B and E8C).

Effect of Torin2 on HALI

To further delineate the role of autophagy upon hyperoxia exposure to epithelial cells and developing lungs, we investigated the effects of Torin2, a pharmacological inhibitor of MTORC1 in hyperoxia settings. Torin2 is a second-generation ATP competitive catalytic inhibitor of MTOR, with 800-fold selectivity over phosphatidylinositol 3-kinases (PtdIns3k) (16). Exposure to hyperoxia led to increased cell death, which was decreased by concomitant treatment by Torin2 (Figure E5; Figures 3A and 3B).

To further confirm the autophagic flux, we performed colocalization puncta experiments using confocal microscopy under different conditions. As expected, characteristic green fluorescent protein (GFP)-LC3 punctate containing autophagosomes were increased in the presence of hyperoxia, as evidenced by yellow and red puncta as compared with diffused GFP-LC3 in the absence of hyperoxia (Figures 3C–3D). In CQ-treated MLE-12 cells, only yellow puncta were found, indicating the blockade of autophagic flux (Figures 3C and 3E). In the case of Torin2-treated MLE-12 cells, yellow and red puncta were found to be further increased, indicating activation of autophagy as compared with its respective control (Figures 3C and 3F).

In complementary *in vivo* experiments, Torin2 administration was found protective of HALI, as evidenced by improved alveolar architecture (Figure 4A), which was confirmed by lung morphometry (Figures 4B and 4C). Next, to gain insight into the mechanism, molecular markers of autophagy and apoptosis pathways were analyzed by Western blotting. As noted in Figure 4D, Torin2 treatment led to a significant decrease in the proapoptotic proteins (active BAX and cleaved CASP3) and significant increase in the autophagy proteins (BECN-1 and LC3-II) upon exposure to hyperoxia. We further confirmed the protective effect of Torin2 in overall survival of NB WT mice in hyperoxia at PN7 (Figure 4F). Taken together, the data corroborate the protective effect of

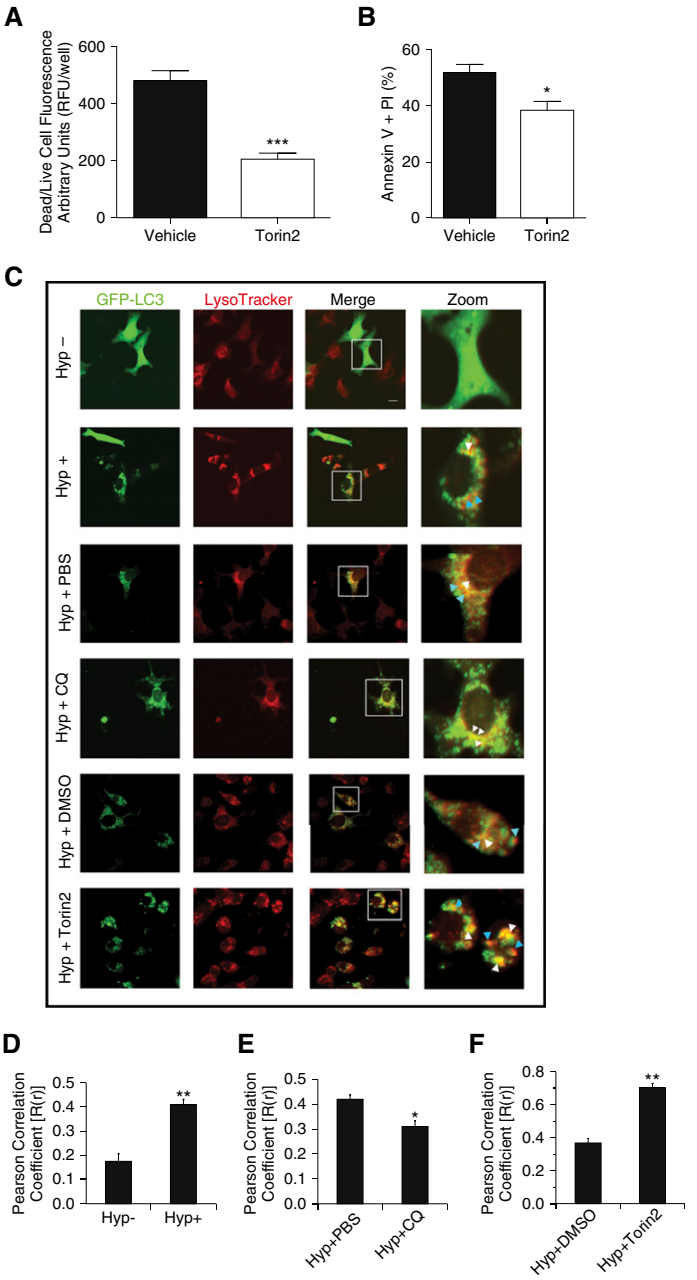

Figure 3. Effect of Torin2 on hyperoxia-induced acute lung injury. (*A*) MLE-12 cells were treated with or without Torin2, exposed to hyperoxia, and dead/live cell fluorescence assay was performed at 24 hours. Quantitative analysis showing significantly decreased dead/live cell fluorescence in the Torin2-treated group compared with control vehicle-treated group (0.1% DMSO) at 24 hours. (*B*) MLE-12 cells were treated with or without Torin2, exposed to hyperoxia, and subjected to annexin V and PI assay. Flow cytometric quantitative analysis showing significantly decreased annexin V– and PI-positive MLE-12 cells of the Torin2-treated group compared with control vehicle-treated group (0.1% DMSO). (*C*) MLE-12 cells transiently expressing green fluorescent protein (GFP)-LC3 were treated with or without CQ (25 μM) and Torin2 (100 nM) and exposed to hyperoxia for 16 and 24 hours, respectively. Formation of acidic vesicular organelles was monitored by LysoTracker deep-red staining, and representative images were obtained using confocal microscopy. *Merge panel* shows the colocalization of punctate GFP-LC3 and LysoTracker staining. Representative LC3-positive early (*yellow*) and late (*red*) autolysosomes were enlarged and marked with *arrows*. *White arrows* indicate yellow puncta; *blue arrows* indicate red puncta. *Scale bar*, 20 μm. (*D–F*) Colocalization was quantified by counting more than 30 cells using Pearson correlation coefficient, and values are represented as means ± SEM of three independent experiments. $^{*}P < 0.05$, $^{**}P < 0.01$, $^{***}P < 0.001$, compared with respective controls.

Torin2 by enhancing cell survival and autophagy markers concomitant with improved HALI and survival in NB WT mice.

Rptor$^{+/-}$ Mouse Lungs Have Increased Autophagy, Decreased Apoptosis, and Improved Pulmonary Architecture upon Hyperoxia Exposure

To specifically delineate the potential effects of *Rptor* deletion in hyperoxia settings, we also used *Rptor* conditional knockout mice using the Cre-Loxp system. To restrict *Rptor* deletion to lung epithelial cells, *Rptor* flox/flox mice were crossed with Nkx2.1 Cre mice.

Hyperoxia exposure to NB *Rptor*$^{-/-}$ mice was found to be universally lethal between PN4 and PN6 (data not shown). However, *Rptor*$^{+/-}$ mice exposed to hyperoxia from PN1–7 showed improved lung morphometry, both in chord length and septal thickness (Figures 5A–5C). Furthermore, there was significantly increased LC3-II, phospho-AKT (S473), phospho-TRP53, phospho-ribosomal protein S6 (RPS6), and significantly decreased RPTOR, phospho-RPS6 kinase beta-1 (RPS6KB1), and cleaved CASP3 in hyperoxia-exposed *Rptor*$^{+/-}$ PN7 mouse lungs (Figures 5D–5F).

In addition, we noted decreased cell proliferation (Ki67 stain) and increased cell death (terminal deoxynucleotidyl transferase dUTP nick end labeling stain) in WT and CQ-treated mice exposed to hyperoxia, which was reversed in *Rptor*$^{+/-}$ and Torin2-treated mice in hyperoxia at PN7 (Figures 5G and 5H). Furthermore, we also colocalized that cell death (using SPC and CASP3) occurred in the type II alveolar cells of the lung (Figure 5I and Figure E10).

Temporal Inhibition of RPTOR Attenuates the BPD Phenotype in Mouse Lungs and Improves PAH-Induced RVH

For the purposes of translational importance, we evaluated the effects of the genetic inhibition of Rptor using specific siRNA. As noted in Figures 6A–6C and Figure E6, a single dose of Rptor siRNA, given before the hyperoxia exposure until PN4 in the developing lungs (saccular stage), was sufficient to protect the lung from impaired alveolarization at PN14. In addition, this protective response was also reflected in the significant reduction of PAH-induced RVH (Figures 6D and 6E). We also noted increased and colocalized LC3-II expression in the *Rptor* siRNA–treated lungs in hyperoxia in the type II alveolar cells of the lung (Figure 6F). In addition, there was significantly increased LC3-II and decreased cleaved CASP3 expression in *Rptor* siRNA–treated, hyperoxia-exposed PN4 mouse lungs (Figure 6G; Figures E7A and E7B). Furthermore, there was significantly increased phospho-Trp53 staining in the *Rptor* siRNA–treated lungs in hyperoxia (Figure 6H). We have suggested a proposed sequence of events to explain the role of autophagy in our models of HALI and BPD (Figure 6I).

Association of LC3 Protein in Human Neonatal Lungs with RDS and BPD

To ascertain the clinical relevance of our findings, we used immunohistochemistry to detect LC3 protein in human neonatal lungs (Table 1). As noted in the representative microphotographs in Figure 7A, there was increased brown staining of the epithelial and inflammatory cells in the lungs of neonates who died later in the course of RDS and BPD. The maximal increase in LC3 staining was noted in the lungs of neonates with RDS greater than PN7 (Figure 7B).

For further confirmation, we used an independent collection of human lung samples matched by gestational and/or PN age (17), and conducted an immunoblot analysis. As noted in Figures 7C and 7D, there was a marked increase in the autophagy marker LC3-II, comparing term control infants with no lung disease to those with established BPD (3). Upon densitometric quantification, it was obvious that the autophagic process increased with severity of disease (as also noted in Figure 7B) and is persistent with established BPD (Figure 7D). Furthermore, we also noted significantly increased phospho-BECN1 and LAMP1, and confirmed the increased LC3-II expression in established BPD using an additional tubulin control (Figures 7E–7H). These data would suggest that hyperoxia and/or ventilation-induced injury to the developing lung are accompanied by activation of the autophagy pathway in human neonates.

Discussion

Provision of supplemental oxygen remains a major clinical intervention for preterm infants with RDS (4). However, administering high concentrations of oxygen can augment lung injury, eventually leading to HALI and BPD (1, 18). Recently, hyperoxia induction of autophagy was found to be regulated by the c-jun-terminal kinase and the Fas-apoptotic pathways (19). Hyperoxia exposure probably leads to the induction of autophagy by reactive oxygen species generation (13). Our previous studies showed the involvement of the c-jun-terminal kinase pathway in hyperoxia-induced cell injury and death in developing lungs (10). Therefore, we sought to investigate the role of autophagy in these processes. In the present study, we show that inhibition of RPTOR, a key accessory protein of multiprotein complex MTORC1, decreases apoptotic cell death by enhancing autophagy in a TRP53-dependent manner in hyperoxia-exposed developing lungs.

We demonstrate increased LC3-II expression, both *in vitro* and *in vivo*, using MLE cells, fetal type II AECs, NB WT mouse lungs, and human lung tissues of neonates with RDS and BPD (Figures 1A–1G and 7A–7H). We also demonstrate that the induction of autophagosome biosynthesis in response to hyperoxia is coupled to autophagic flux in MLE cells and in human lung samples (Figures 2A and 2B, 3C–3F, and 7E–7H) (20–22). Because TRP53 activation is noted concomitant with increased autophagy (Figures 1A–1D), we explored their relationship in hyperoxic conditions. Using pharmacological inhibitors, CQ and pifithirin-α, as well as *Trp53*-specific gene knockdown, we demonstrated hyperoxia-induced autophagic flux is *Trp53* dependent in MLE-12 cells (Figure E1; Figures 2C and 2D) and in mouse lungs (Figure 2K; Figure E8D). In support of this, there are prior studies demonstrating activation of autophagy pathway in a *Trp53*-dependent manner (23–25). Our data of TRP53 phosphorylation at S392 and acetylation at K379 as evidence of TRP53 activation is supported by other investigators who have reported that *Trp53* transcription of genes is critical for many biologic processes, including autophagy (26, 27). It has also been reported that ULK1 is a

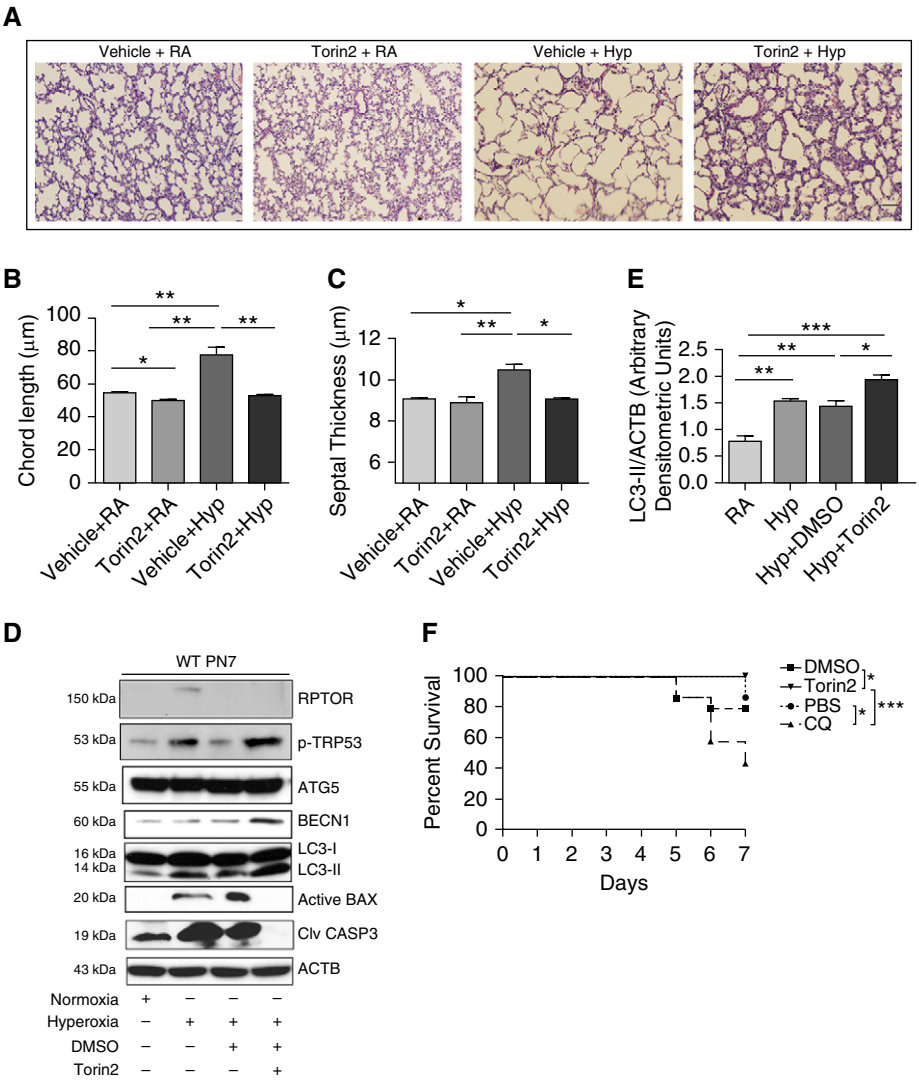

Figure 4. Torin2 treatment decreased apoptosis and improved lung morphometry and overall survival. (*A*) Representative images of lung histology (hematoxylin and eosin [H&E] stain) of NB WT mice treated with Torin2 (20 mg/kg; twice daily) and exposed to RA or 100% O_2 and survived till PN7. *Scale bar*, 100 μm. (*B* and *C*) Morphometric analyses of lung histology sections of NB WT mice exposed to RA or survived 100% O_2 at PN7. Alveolar size expressed as chord length, and septal thickness were analyzed using Image J software (National Institutes of Health, Bethesda, MD). (*D*) Western blot analysis of regulatory-associated protein of mechanistic target of rapamycin (RPTOR), TRP53, ATG5, BECN1, LC3-II, proapoptotic active Bax, and cleaved caspase (CASP) 3 was performed on total lungs obtained from NB WT mice treated with Torin2 and exposed to RA or hyperoxia until PN7. (*E*) Densitometric analysis was performed and the expression of LC3-II was normalized to ACTB. (*F*) Effect of Torin2 and CQ on survival of NB WT mice in hyperoxia at PN7. Survival data showing 100% survival of Torin2-treated NB WT mice exposed to hyperoxia, at PN7. NB WT and CQ-treated mice had 85 and 42.8% survival rates, respectively, at PN7. A minimum of 10 animals was used in each group. Values are means ± SEM of a minimum of three observations (*in vitro* experiments) or four animals (*in vivo* experiments). $^{*}P < 0.05$, $^{**}P < 0.01$, $^{***}P < 0.001$, ANOVA. DMSO, vehicle for Torin2; PBS, vehicle for CQ.

transcriptional target of TRP53 and thereby up-regulates autophagy (28).

Work by other investigators has reported increased survival of hyperoxia-exposed A549 cells by activation of autophagy after exposure to carbon monoxide (13). Using Beas-2B cells, hyperoxia-induced autophagy ablated apoptosis initiation through the Fas-dependent death signaling pathway (19). Finally, using hyperoxia-exposed primary cultures of AECs from adult mouse lungs, sequestosome 1 (SQSTM1)/p62/LC3-II complex was found to regulate cell survival (29). It is important to clarify the relationship between the increased levels of SQSTM1 expression and increased autophagy signaling in hyperoxia-exposed MLE-12 cells and neonatal mouse systems that we have noted (Figures 1A–1D). There is general consensus that increased levels of this multifunctional protein, SQSTM1, serves as a readout of autophagic degradation (14). However, the role of SQSTM1 in the course of hyperoxia-induced autophagy has been documented to have a protective role in lung epithelial cells (29).

We found increased phospho-RPS6KB1 and phospho-RPS6 indicating MTORC1 activity upon hyperoxia exposure in our model systems. Adenoviral-mediated transduction of *Akt* led to increased phospho-RPS6KB1 expression upon hyperoxia exposure in human lung microvascular endothelial cells (HLMVECs), and was considered protective against hyperoxia stress (30). In HLMVECs, hyperoxia exposure increased extracellular adenosine triphosphate at 30 minutes; within the same time frame, ATP treatment induced phosphorylation of RPS6KB1, which is downstream of MTORC1 (31). When HLMVECs were exposed to hyperoxia for 48 hours, there appears to be no change in phospho-MTOR and phospho-RPS6KB1 (30). However, MTOR inhibition by rapamycin enhanced HLMVEC death when exposed to hyperoxia for 6 days. In our experiments, inhibition of MTORC1 led to decreased cell death upon exposure to hyperoxia (Figures 4A and 4B). This difference in results could be secondary to cell specificity.

Nutrient depletion in a multiple myeloma cell line (RPM18226) induced autophagy (BECN1 dependent, and related to MTORC1 inhibition) maximally by 18 hours, which declined at 24 and 48 hours, whereas apoptosis (caspase-3 mediated and BAX dependent) continued to increase until 48 hours (32). Thus, autophagy protected against apoptosis, at least initially, and in addition, Sirtuin-1 (Sirt1) appeared to contribute to this protective response (32). Interestingly, we have recently reported that low Sirt1 lung cellular (tracheal aspirate leukocytes) concentrations in human neonates were associated with an increased

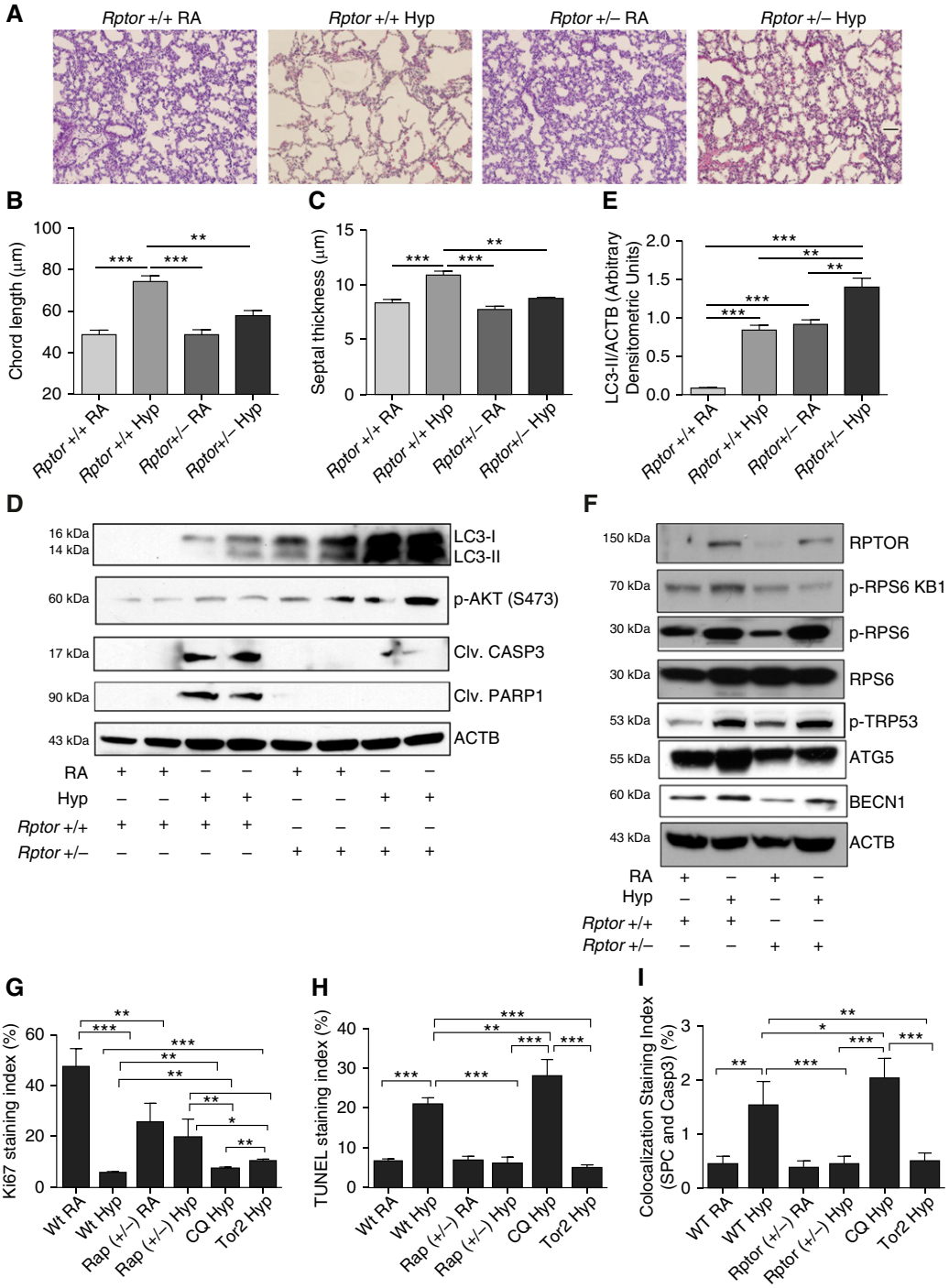

Figure 5. *Rptor*$^{+/-}$ mice demonstrated decreased apoptosis and improved lung morphometry. (*A*) Representative images of lung histology (H&E stain) of NB *Rptor*$^{+/-}$ mice exposed to RA or 100% O_2 at PN7. *Scale bar*, 100 μm. (*B* and *C*) *Bar graphs* showing the morphometric analysis of lung histology sections of NB *Rptor*$^{+/-}$ mice exposed to RA or 100% O_2 at PN7. (*D*) Western blot analysis of phospho-AKT, cleaved CASP3, cleaved poly ADP ribose polymerase 1 (PARP1), and LC3-II was performed on total lung homogenates obtained from NB *Rptor*$^{+/-}$ mice exposed to RA or 100% O_2 at PN7. (*E*) Densitometric analysis of LC3-II normalized to ACTB. (*F*) Western blot analysis of RPTOR, phospho-RPS6, RPS6, ATG5, BECN1, and phospho-TRP53 was performed on total lung homogenates obtained from NB *Rptor*$^{+/-}$ mice exposed to RA or 100% O_2 at PN7. (*G*) *Bar graph* showing the colocalization staining index (Ki67 and SPC) between WT RA, WT Hyp, *Rptor*$^{+/-}$ RA, *Rptor*$^{+/-}$ Hyp, CQ Hyp, and Torin2 Hyp groups, respectively. (*H*) *Bar graph* showing the TUNEL staining index between WT RA, WT Hyp, *Rptor*$^{+/-}$ RA, *Rptor*$^{+/-}$ Hyp, CQ Hyp, and Torin2 Hyp groups, respectively. (*I*) *Bar graph* showing the colocalization staining index of SPC and CASP3 between WT RA, WT Hyp, *Rptor*$^{+/-}$ RA, *Rptor*$^{+/-}$ Hyp, CQ Hyp, and Torin2 Hyp groups, respectively. Values are means ± SEM of a minimum of four animals used in each group. *$P < 0.05$, **$P < 0.01$, ***$P < 0.001$, ANOVA. *Rptor*$^{+/+}$, C57BL/6J control mice (same as *Rptor* strain); *Rptor*$^{+/-}$, *Rptor* heterozygous mice.

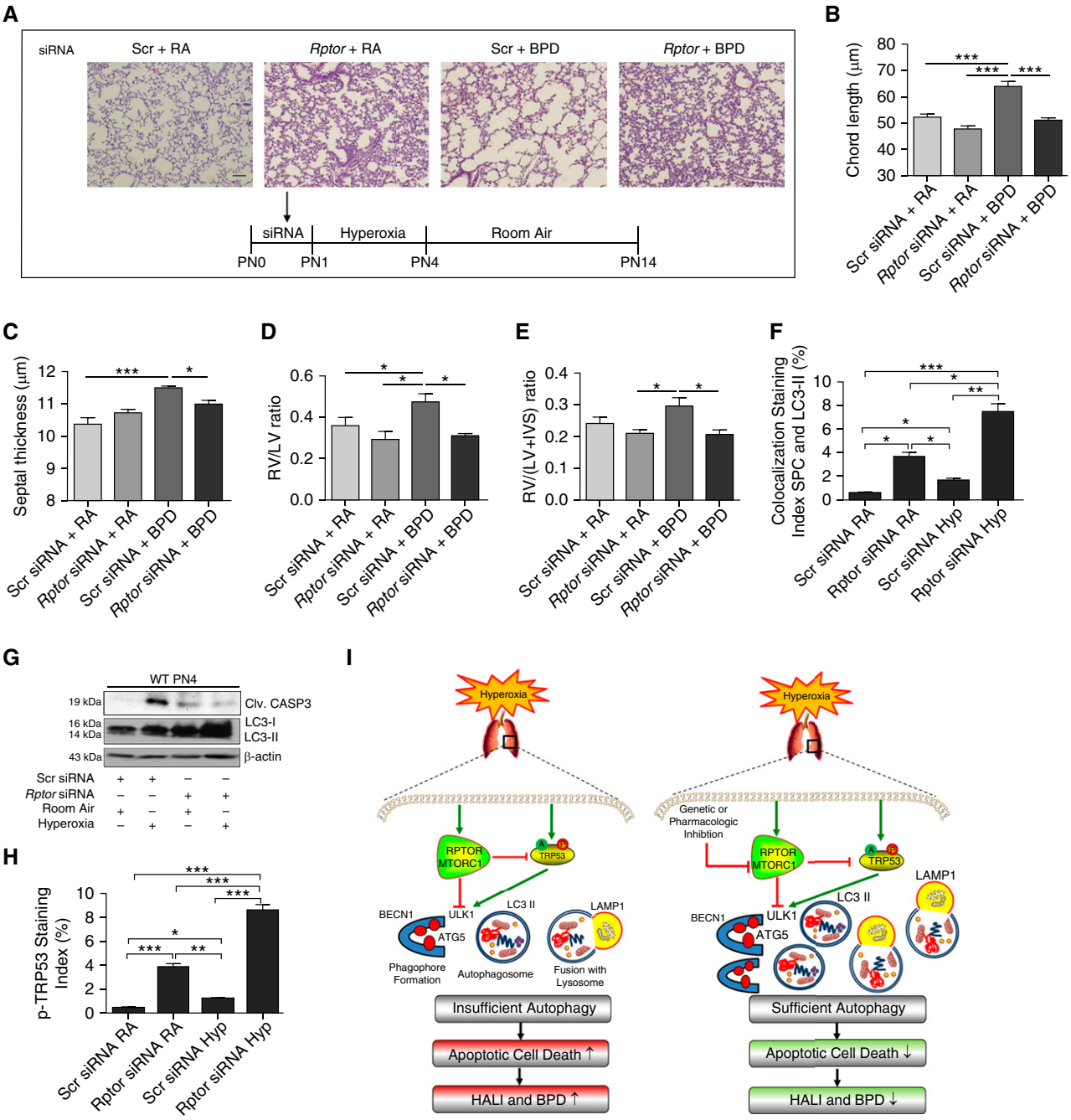

Figure 6. Temporal inhibition of *Rptor* attenuates bronchopulmonary dysplasia (BPD) phenotype in mouse lungs and improves pulmonary arterial hypertension–induced right ventricular (RV) hypertrophy in mouse hearts. (*A*) Representative H&E stain images depicting lung histology. *Rptor* siRNA was administered intranasal to PN0–PN1 mice at room air and then exposed to 100% O_2 between PN1–PN4 followed by recovery until PN14 at room air. *Scale bar*, 100 μm. (*B* and *C*) *Bar graphs* showing the morphometric analysis of lung histology sections of NB WT mice treated with *Rptor* siRNA and exposed to hyperoxia followed by recovery at room air until PN14. (*D* and *E*) *Bar graphs* showing the ventricular free wall thickness as indicated by RV to left ventricle (LV) ratio and RV hypertrophy, as indicated by RV/(LV + interventricular septum) at PN14. (*F*) *Bar graph* showing the co-localization staining index of SPC and LC3-II in *Rptor* siRNA–treated and exposed to hyperoxia until PN4. (*G*) Western blotting showing increased expression of LC3-II and decreased expression of cleaved CASP3 in *Rptor* siRNA–treated, hyperoxia-exposed PN4 mouse lungs. (*H*) *Bar graph* showing the phospho-TRP53 staining index of *Rptor* siRNA–treated mouse lungs exposed to hyperoxia until PN4. (*I*) *Schema* representing the proposed mechanism is illustrated. The *left panel* shows that concomitant increase in MTOR complex (MTORC) 1 and TRP53 activation in the developing lung upon hyperoxia exposure. Activation of TRP53 led to increased autophagy. However, this increased autophagy was insufficient, due to the inhibitory role of MTORC1, and is associated with increased apoptotic cell death and leads to hyperoxia-induced acute lung injury (HALI) and BPD. The *right panel* shows that, when a key subunit of MTORC1, RPTOR, is inhibited, a further increase in autophagy is noted, leading to decreased apoptotic cell death, which has a protective effect and attenuates HALI and BPD. Values are means ± SEM of a minimum of four animals used in each group. $^*P < 0.05$, $^{**}P < 0.01$, $^{***}P < 0.001$, ANOVA.

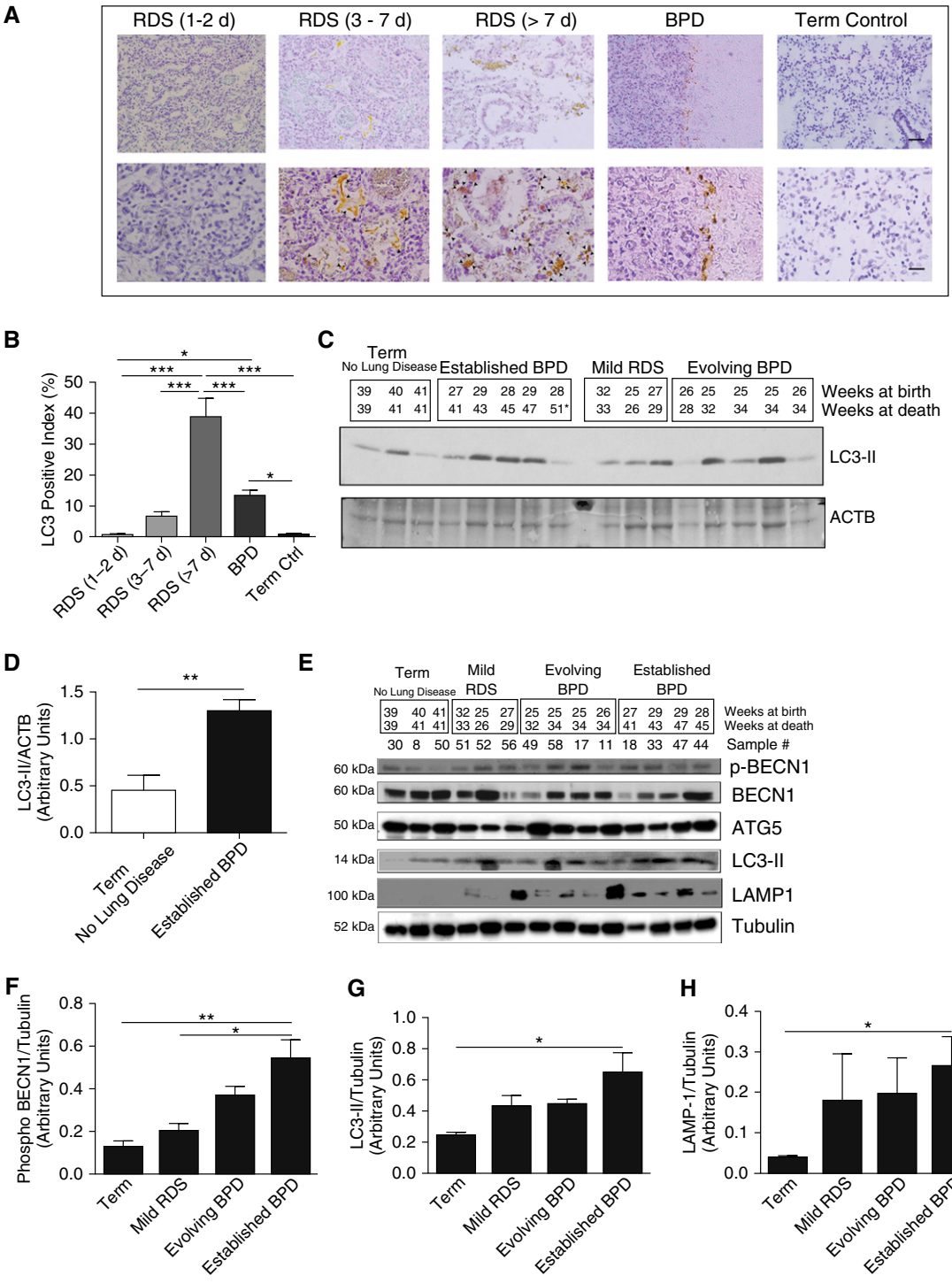

Figure 7. Association of LC3 protein in human neonatal lungs with RDS and BPD. (*A*) Representative immunohistochemistry images showing increased staining of LC3 protein expression in samples from patients with RDS and BPD. *Upper scale bar*, 100 μm; *bottom scale bar*, 20 μm. (*B*) Quantitative analysis in a representative graph showing increased LC3-positive index of lung samples from patients with RDS and BPD. Values are means ± SEM of two to three patients in each group. $^{*}P < 0.05$, $^{***}P < 0.001$. (*C*) Western blot analysis of LC3-II expression was performed on total lung homogenates from human lung samples. Gestational age at birth and death are indicated. (*D*) Densitometric analysis of samples from infants born at term with no lung disease as compared with term with established BPD as primary cause of death. (*E*) Western blot analysis of phospho-BECN1, total BECN1, ATG5, LC3-II, and LAMP1 expression was performed on total homogenates from human lung samples (note: we excluded one infant dying at 51 wk from the densitometry analysis because his pathology and clinical status at death suggested resolved BPD, with the cause of death being recurrent necrotizing enterocolitis). (*F–H*) Densitometric analysis of phospho-BECN1, LC3-II, and LAMP1 expression from infants born near term with no lung disease as compared with near or postterm with mild RDS, evolving BPD, and established BPD as primary cause of death. $^{*}P < 0.05$, $^{**}P < 0.01$, ANOVA. RDS, respiratory distress syndrome.

Table 1. Selected Clinical Data of Infants Whose Lungs Were Used for the Immunohistochemical Analyses for Light Chain-3 Protein

Diagnosis	Gestational Age (*Wk*)	Birth Weight (*g*)	Age at Death (*d*)
RDS 1–2 d	25 + 5	500	2
RDS 1–2 d	25 + 0	410	2
RDS 3–7 d	30 + 3	1,430	3
RDS 3–7 d	26 + 1	750	4
RDS 3–7 d	23 + 6	700	3
RDS >7 d	23 + 5	610	11
RDS >7 d	27 + 0	540	13
BPD	26 + 6	890	79
BPD	29	765	125
BPD	29	1,070	175
Term	41	4,300	3
Term	37	2,800	4 h

Definition of abbreviations: BPD, bronchopulmonary dysplasia; RDS, respiratory distress syndrome.

likelihood of BPD or death (33). We can speculate of a possible mechanistic contributory role of Sirt1 in BPD via the autophagy-apoptotic signaling pathway.

Many studies have been described that MTORC1 acts a negative regulator of autophagy by suppressing ULK1 at the nucleation stage of autophagy (34, 35). In the current study, we explored pathway relationships between MTORC1, TRP53, autophagy and apoptosis in hyperoxia exposed developing lungs.

Using gene knockdown experiments and specific inhibitors of autophagy, we were able to demonstrate increased apoptosis when autophagy is inhibited (by *Atg5*, *Becn1*, *Map1lc3/lc3* and *Lamp1* siRNAs and CQ) (Figure E3; Figures 2E–2H) or decreased apoptosis when autophagy is enhanced by Torin2 during hyperoxia exposure (Figures 3A and 3B). In accord with our data, inhibition of autophagy by CQ has been shown to enhance apoptotic cell death in BCR-ABL expressing leukemic cells. Providing supportive evidence *in vivo*, we administered CQ to hyperoxia exposed NB WT PN7 mice and demonstrated significantly increased chord length, increased active BAX and CASP-dependent apoptotic cell death (Figures 2H, Figures E4 and E8). It is worth noting that administration of Torin2 to hyperoxia-exposed NB WT PN7 mice protected from apoptotic cell death and improved lung architecture (Figures 4A–4D). In addition, Torin2-treated mice did not show any alteration in terms of systemic growth as compared with untreated mice. It is worth investigating the potential effect of Torin2 on the immune system and inflammation, as neonatal mice are considered immunodeviant (36). Survival data showed significantly decreased survival in the CQ-treated group; conversely, the Torin2-treated group had 100% survival upon exposure to hyperoxia (Figure 4F). Given the importance of enhancing autophagy as therapeutic intervention in hyperoxia-induced lung injury, we also used *Rptor* conditional knockout mice. Upon hyperoxia exposure, homozygous deletion of *Rptor* was found to be universally lethal, suggesting minimal levels required for homeostasis. However, NB *Rptor*$^{+/-}$ PN7 mice exposed to hyperoxia showed significantly decreased apoptosis, increased autophagy, and improved lung architecture (Figures 5A–5F). Interestingly, phospho-TRP53 was found to be increased in addition to increased expression of LC3-II, phospho-AKT, and phospho-RPS6 in NB Rptor$^{+/-}$ PN7 mice (Figures 5D–5F). In accordance with this observation, a recent paper demonstrated that MTOR hypomorphic mice, which express MTOR at only 25% of WT controls, displayed increased overall lifespan (37). However, our data demonstrated that inhibition of *Rptor* plays a protective role in pulmonary epithelial cells, it is worth investigating the effect of *Rptor* inhibition in pulmonary endothelial cells, a cell type sensitive to hyperoxia exposure. Taken together, our data confirm inhibition of RPTOR acts as a potential therapeutic target to decrease apoptotic cell death in developing lungs exposed to hyperoxia.

Endoplasmic reticulum stress induced autophagy in an adult diabetes rodent model; conversely, inhibition of autophagy induced apoptosis (38). Enhancement of autophagy by MTORC1 inhibition prevented apoptosis and improved diabetic phenotype (38). In contrast, we have recently reported that endoplasmic reticulum stress in hyperoxia- and IFN-γ–induced mouse models of BPD was associated with increased apoptotic cell death, although no data on autophagy were reported (39). In breast cancer lines, IFN-β induced autophagy upstream of MTORC1, whereas the proapoptotic function was significantly increased in the absence of autophagy (40). In such a scenario, inhibition of autophagy would be considered clinically more important. In contrast, silencing of lung endothelial heme oxygenase-1 enhanced hyperoxia-induced mitochondrial oxidant generation and inhibition of autophagy, which ultimately increased apoptosis in adult mice (41). Because heme oxygenase-1 is considered a critical protective molecule against HALI, one could speculate that enhancing autophagy would be beneficial by decreasing apoptosis and protecting against HALI in adult mice (41). This would be in accord with our results, wherein enhancing autophagy prevented apoptotic cell death upon hyperoxia exposure in lung epithelial cells and protected against HALI in neonatal mice.

To mimic the context of BPD in human neonates, neonatal mice were administered a genetic inhibitor of *Rptor* before hyperoxia exposure for 4 days. Our data suggest that temporal inhibition of *Rptor* led to increased LC3-II, decreased cleaved CASP3, improved lung architecture, and PAH-induced RVH (Figures 6A–6G; Figures E7A and E7B). In accord with our data, sildenafil treatment of a two-hit model of BPD in which NB rat pups were exposed to prenatal LPS followed by PN hyperoxia exposure for 1 week and/or recovery in room air for another week, had improved alveolarization, both at PN7 and PN14 (42).

In hyperoxia settings, our results suggest that loss of RPTOR leads to an increase in the survival factor, phospho-AKT. We speculate that this could be a downstream effect of a compensatory increase in MTORC2 upon partial inhibition of MTORC1. On the other

hand, we demonstrated increased LC3-II in addition to increased phospho-BECN1 and increased LAMP1 expression, suggesting altered autophagy flux in human neonates with BPD (Figures 7A–7H). However, it is important to emphasize that the increase in autophagy markers is an associated finding in lungs of human neonates with RDS and BPD, but not confirmatory that the autophagy has a protective or contributory role. Thus, we have demonstrated that, in both acute (HALI) and chronic (BPD) hyperoxia-induced injury scenarios, enhancing autophagy by inhibiting RPTOR has beneficial antiapoptotic effects in developing lungs. In sharp contrast, MTOR inhibition has been shown to increase LPS-induced lung injury and apoptosis in adult mice (43). This suggests both stress- and developmental stage–specific signaling pathways are responsible for differences in neonatal compared with adult mice. This highlights the importance of independent testing of hyperoxia or other modes of injury stimuli and intervention approaches in developmentally appropriate models to elucidate the uniqueness of the response in the NB lung for the clinical context of neonatal-specific diseases, rather than extrapolating from adult studies (18, 44, 45).

In conclusion, our study provides novel mechanistic information by which autophagy participates to limit apoptosis as an inherent protective response after hyperoxia exposure in developing lungs. Enhancement of this protective response by selective inhibition of RPTOR resulted in sufficient levels of autophagy and led to decreased apoptotic cell death, improved lung architecture, and increased survival in developing lungs exposed to hyperoxia. Our data suggest that, in addition to supplemental oxygen, increasing autophagy by selective inhibition of RPTOR may act as a potential therapeutic target for the prevention of HALI and BPD in neonates. ■

Author disclosures are available with the text of this article at www.atsjournals.org.

References

1. Bhandari V. Hyperoxia-derived lung damage in preterm infants. *Semin Fetal Neonatal Med* 2010;15:223–229.
2. Bhandari A, Bhandari V. "New" bronchopulmonary dysplasia—a clinical review. *Clin Pulm Med* 2011;18:137–143.
3. Bhandari A, Bhandari V. Pitfalls, problems, and progress in bronchopulmonary dysplasia. *Pediatrics* 2009;123:1562–1573.
4. Bhandari V, Choo-Wing R, Lee CG, Zhu Z, Nedrelow JH, Chupp GL, Zhang X, Matthay MA, Ware LB, Homer RJ, *et al*. Hyperoxia causes angiopoietin 2–mediated acute lung injury and necrotic cell death. *Nat Med* 2006;12:1286–1293.
5. Mizushima N, Levine B. Autophagy in mammalian development and differentiation. *Nat Cell Biol* 2010;12:823–830.
6. Sridhar S, Botbol Y, Macian F, Cuervo AM. Autophagy and disease: always two sides to a problem. *J Pathol* 2012;226:255–273.
7. Lipinski MM, Hoffman G, Ng A, Zhou W, Py BF, Hsu E, Liu X, Eisenberg J, Liu J, Blenis J, *et al*. A genome-wide siRNA screen reveals multiple mTORC1 independent signaling pathways regulating autophagy under normal nutritional conditions. *Dev Cell* 2010;18:1041–1052.
8. Martina JA, Chen Y, Gucek M, Puertollano R. MTORC1 functions as a transcriptional regulator of autophagy by preventing nuclear transport of TFEB. *Autophagy* 2012;8:903–914.
9. Huang Z, Wang Y, Nayak PS, Dammann CE, Sanchez-Esteban J. Stretch-induced fetal type II cell differentiation is mediated via ErbB1–ErbB4 interactions. *J Biol Chem* 2012;287:18091–18102.
10. Li Z, Choo-Wing R, Sun H, Sureshbabu A, Sakurai R, Rehan VK, Bhandari V. A potential role of the JNK pathway in hyperoxia-induced cell death, myofibroblast transdifferentiation and TGF-β1–mediated injury in the developing murine lung. *BMC Cell Biol* 2011;12:54.
11. Harijith A, Choo-Wing R, Cataltepe S, Yasumatsu R, Aghai ZH, Janér J, Andersson S, Homer RJ, Bhandari V. A role for matrix metalloproteinase 9 in IFNγ-mediated injury in developing lungs: relevance to bronchopulmonary dysplasia. *Am J Respir Cell Mol Biol* 2011;44:621–630.
12. Sun H, Choo-Wing R, Sureshbabu A, Fan J, Leng L, Yu S, Jiang D, Noble P, Homer RJ, Bucala R, *et al*. A critical regulatory role for macrophage migration inhibitory factor in hyperoxia-induced injury in the developing murine lung. *PLoS One* 2013;8:e60560.
13. Lee SJ, Ryter SW, Xu JF, Nakahira K, Kim HP, Choi AM, Kim YS. Carbon monoxide activates autophagy via mitochondrial reactive oxygen species formation. *Am J Respir Cell Mol Biol* 2011;45:867–873.
14. Klionsky DJ, Abdalla FC, Abeliovich H, Abraham RT, Acevedo-Arozena A, Adeli K, Agholme L, Agnello M, Agostinis P, Aguirre-Ghiso JA, *et al*. Guidelines for the use and interpretation of assays for monitoring autophagy. *Autophagy* 2012;8:445–544.
15. Patel AS, Morse D, Choi AM. Regulation and functional significance of autophagy in respiratory cell biology and disease. *Am J Respir Cell Mol Biol* 2013;48:1–9.
16. Liu Q, Wang J, Kang SA, Thoreen CC, Hur W, Ahmed T, Sabatini DM, Gray NS. Discovery of 9-(6-aminopyridin-3-yl)-1-(3-(trifluoromethyl) phenyl)benzo[h][1,6]naphthyridin-2(1H)-one (Torin2) as a potent, selective, and orally available mammalian target of rapamycin (mTOR) inhibitor for treatment of cancer. *J Med Chem* 2011;54: 1473–1480.
17. Bhattacharya S, Go D, Krenitsky DL, Huyck HL, Solleti SK, Lunger VA, Metlay L, Srisuma S, Wert SE, Mariani TJ, *et al*. Genome-wide transcriptional profiling reveals connective tissue mast cell accumulation in bronchopulmonary dysplasia. *Am J Respir Crit Care Med* 2012;186:349–358.
18. Bhandari V. Molecular mechanisms of hyperoxia-induced acute lung injury. *Front Biosci* 2008;13:6653–6661.
19. Tanaka A, Jin Y, Lee SJ, Zhang M, Kim HP, Stolz DB, Ryter SW, Choi AM. Hyperoxia-induced LC3B interacts with the Fas apoptotic pathway in epithelial cell death. *Am J Respir Cell Mol Biol* 2012;46:507–514.
20. Russell RC, Tian Y, Yuan H, Park HW, Chang YY, Kim J, Kim H, Neufeld TP, Dillin A, Guan KL. ULK1 induces autophagy by phosphorylating Beclin-1 and activating VPS34 lipid kinase. *Nat Cell Biol* 2013;15: 741–750.
21. Agrawal V, Jaiswal MK, Mallers T, Katara GK, Gilman-Sachs A, Beaman KD, Hirsch E. Altered autophagic flux enhances inflammatory responses during inflammation-induced preterm labor. *Sci Rep* 2015;5:9410.
22. Bayod S, Del Valle J, Pelegri C, Vilaplana J, Canudas AM, Camins A, Jimenez A, Sanchez-Roige S, Lalanza JF, Escorihuela RM, Pallas M. Macroautophagic process was differentially modulated by long-term moderate exercise in rat brain and peripheral tissues. *J Physiol Pharmacol* 2014;65:229–239.
23. Farnebo M, Bykov VJ, Wiman KG. The p53 tumor suppressor: a master regulator of diverse cellular processes and therapeutic target in cancer. *Biochem Biophys Res Commun* 2010;396:85–89.
24. Scherz-Shouval R, Weidberg H, Gonen C, Wilder S, Elazar Z, Oren M. p53-dependent regulation of autophagy protein LC3 supports cancer cell survival under prolonged starvation. *Proc Natl Acad Sci USA* 2010;107:18511–18516.
25. Tasdemir E, Maiuri MC, Galluzzi L, Vitale I, Djavaheri-Mergny M, D'Amelio M, Criollo A, Morselli E, Zhu C, Harper F, *et al*. Regulation of autophagy by cytoplasmic p53. *Nat Cell Biol* 2008;10:676–687.
26. Beckerman R, Prives C. Transcriptional regulation by p53. *Cold Spring Harb Perspect Biol* 2010;2:a000935.
27. Keller DM, Zeng X, Wang Y, Zhang QH, Kapoor M, Shu H, Goodman R, Lozano G, Zhao Y, Lu H. A DNA damage–induced p53 serine 392 kinase complex contains CK2, hSpt16, and SSRP1. *Mol Cell* 2001;7: 283–292.

28. Gao W, Shen Z, Shang L, Wang X. Upregulation of human autophagy-initiation kinase ULK1 by tumor suppressor p53 contributes to DNA-damage–induced cell death. *Cell Death Differ* 2011;18:1598–1607.
29. Liang X, Wei SQ, Lee SJ, Fung JK, Zhang M, Tanaka A, Choi AM, Jin Y. p62 sequestosome 1/light chain 3b complex confers cytoprotection on lung epithelial cells after hyperoxia. *Am J Respir Cell Mol Biol* 2013;48:489–496.
30. Ahmad A, Ahmad S, Chang LY, Schaack J, White CW. Endothelial Akt activation by hyperoxia: role in cell survival. *Free Radic Biol Med* 2006;40:1108–1118.
31. Ahmad S, Ahmad A, Ghosh M, Leslie CC, White CW. Extracellular ATP–mediated signaling for survival in hyperoxia-induced oxidative stress. *J Biol Chem* 2004;279:16317–16325.
32. Zeng R, He J, Peng J, Chen Y, Yi S, Zhao F, Cui G. The time-dependent autophagy protects against apoptosis with possible involvement of Sirt1 protein in multiple myeloma under nutrient depletion. *Ann Hematol* 2012;91:407–417.
33. Mody K, Saslow JG, Kathiravan S, Eydelman R, Bhat V, Stahl GE, Pyon K, Bhandari V, Aghai ZH. Sirtuin1 in tracheal aspirate leukocytes: possible role in the development of bronchopulmonary dysplasia in premature infants. *J Matern Fetal Neonatal Med* 2012; 25:1483–1487.
34. Kim YM, Jung CH, Seo M, Kim EK, Park JM, Bae SS, Kim DH. mTORC1 phosphorylates UVRAG to negatively regulate autophagosome and endosome maturation. *Mol Cell* 2015;57:207–218.
35. Choi AM, Ryter SW, Levine B. Autophagy in human health and disease. *N Engl J Med* 2013;368:1845–1846.
36. Basha S, Surendran N, Pichichero M. Immune responses in neonates. *Expert Rev Clin Immunol* 2014;10:1171–1184.
37. Wu JJ, Liu J, Chen EB, Wang JJ, Cao L, Narayan N, Fergusson MM, Rovira II, Allen M, Springer DA, *et al*. Increased mammalian lifespan and a segmental and tissue-specific slowing of aging after genetic reduction of mTOR expression. *Cell Reports* 2013;4:913–920.
38. Bachar-Wikstrom E, Wikstrom JD, Kaiser N, Cerasi E, Leibowitz G. Improvement of ER stress–induced diabetes by stimulating autophagy. *Autophagy* 2013;9:626–628.
39. Choo-Wing R, Syed MA, Harijith A, Bowen B, Pryhuber G, Janér C, Andersson S, Homer RJ, Bhandari V. Hyperoxia and interferon-γ–induced injury in developing lungs occur via cyclooxygenase-2 and the endoplasmic reticulum stress–dependent pathway. *Am J Respir Cell Mol Biol* 2013;48:749–757.
40. Ambjørn M, Ejlerskov P, Liu Y, Lees M, Jäättelä M, Issazadeh-Navikas S. IFNB1/interferon-β–induced autophagy in MCF-7 breast cancer cells counteracts its proapoptotic function. *Autophagy* 2013;9: 287–302.
41. Zhang Y, Jiang G, Sauler M, Lee PJ. Lung endothelial HO-1 targeting *in vivo* using lentiviral miRNA regulates apoptosis and autophagy during oxidant injury. *FASEB J* 2013;27:4041–4058.
42. Park HS, Park JW, Kim HJ, Choi CW, Lee HJ, Kim BI, Chun YS. Sildenafil alleviates bronchopulmonary dysplasia in neonatal rats by activating the hypoxia-inducible factor signaling pathway. *Am J Respir Cell Mol Biol* 2013;48:105–113.
43. Fielhaber JA, Carroll SF, Dydensborg AB, Shourian M, Triantafillopoulos A, Harel S, Hussain SN, Bouchard M, Qureshi ST, Kristof AS. Inhibition of mammalian target of rapamycin augments lipopolysaccharide-induced lung injury and apoptosis. *J Immunol* 2012;188:4535–4542.
44. Choo-Wing R, Nedrelow JH, Homer RJ, Elias JA, Bhandari V. Developmental differences in the responses of IL-6 and IL-13 transgenic mice exposed to hyperoxia. *Am J Physiol Lung Cell Mol Physiol* 2007;293:L142–L150.
45. Bhandari V, Choo-Wing R, Lee CG, Yusuf K, Nedrelow JH, Ambalavanan N, Malkus H, Homer RJ, Elias JA. Developmental regulation of NO-mediated VEGF-induced effects in the lung. *Am J Respir Cell Mol Biol* 2008;39:420–430.